3D Particle Tracking on the Two-Photon Microscope

Tim Ragan[a], Peter T. So[b], Hyuk-Sang Kwon[b], and Enrico Gratton[a]

[a]Department of Physics, University of Illinois at Urbana-Champaign, Urbana IL
[b]Department of Mechanical Engineering, Massachusetts Institute of Technology, Cambridge, MA

ABSTRACT

We have developed a 3D single-particle-tracking (SPT) system based around the two-photon laser-scanning fluorescence microscope that can track particles in all three dimensions and at a high frequency response. We have implemented two different techniques to achieve this goal. The techniques employ feedback control in order to track the particle but differ in the approach they use to ascertain the particle's 3D position. The first technique scans a small volume around a particle to build up a volumetric image that is then used to determine the particle position. The second technique scans only a single plane but utilizes optical aberrations which have been introduced into the optical system that break the axial symmetry of the point spread function and serves as an indicator of the particle's axial position. The current system has a frequency response at the video rate and an axial range of 100 μm. We tested the system by tracking well-defined test trajectories, and by tracking particles in model systems. We identified several different modes of motion in sucrose solutions and agarose gels, including the transient trapping of particles in the microdomains of agarose gels.

Keywords: Single particle tracking, two-photon microscopy, 3D imaging

1.Introduction

Single particle tracking (SPT) is an optical microscopy technique where the motion of a single particle is followed. The first paper describing SPT was by Barak and Webb[1], which used SPT to trace the motion of fluorescently tagged low-density lipoprotein receptors in the plasma membrane of human fibroblasts. The technique was extended to both bright field and differential interference contrast microscopy and used to follow the motion of gold particles[2,3].

SPT has several strengths that makes it an attractive technique for use in biological research. First, SPT possesses a spatial resolution as high as five nanometers. In contrast, a technique such as FRAP (fluorescence recovery after photobleaching) is limited to the dimensions of the point-spread function (PSF) (~0.5 μm). Second, SPT has a fast temporal resolution. Many of the experiments have been done at the video rate (33 Hz) and some have achieved kinetics as fast as 200 Hz[4]. Another advantage of SPT is that experiments can be done in-vivo. Besides being nondestructive, in-vivo studies also allow the biochemical microenvironment around the particle to be probed. In addition, by its very nature, SPT allows the motion of individual particles to be studied rather than the ensemble averaged behavior of a population of particles. This can provide much more detailed information than other techniques can, particularly when dealing with heterogeneous populations. For example, SPT has helped reveal the different sub-populations of receptor molecules in the plasma membrane[5].

SPT has some technical challenges: there can be artifacts due to labeling the particle with a relatively large latex or gold sphere; ambiguities may arise in the interpretation of the trajectories of particles; photobleaching or low signal to noise ratios can be a factor with fluorescent probes; and for high spatial resolution studies (~10 nm), it may be necessary to mechanically isolate the instrument from vibrations.

The early SPT systems were all two-dimensional systems. These systems were not able to effectively address fundamentally 3D phenomena such as endocytosis, intracellular transport and diffusion within the cytoplasm. To address this limitation, research groups have developed some 3D SPT tracking systems. Kao and Verkman[6] developed a 3D SPT system that employed cylindrical optics in order to break the axial symmetry of the PSF and thus enable 3D single particle tracking. They obtained a frequency response of 3-4 Hz and resolution of 12 nm in the axial direction and 5 nm in the radial direction. Peters *et al.*[7] who monitored the position of a laser beam focused onto a polystyrene sphere in order to track a particle in 3D. They were able to obtain a 1 kHz frequency response with an accuracy of 1 nm. Pralle *et al.*[8] used a quadrant photodiode to detect the scattered light from a trapped sphere for 3D tracking. This technique has a high spatial and temporal resolution but a fairly limited range and calibrations are required for different axial depths.

Multiphoton Microscopy in the Biomedical Sciences, Ammasi Periasamy, Peter T. C. So, Editors,
Proceedings of SPIE Vol. 4262 (2001) © 2001 SPIE · 1605-7422/01/$15.00

Two-photon excitation is an excited state transition caused by the simultaneous absorption of two photons. Its application to microscopy was first implemented by Denk *et al.*[9]. Since the excitation goes as the second power of the laser intensity in two-photon microscopy, appreciable excitation occurs only near the focal plane where the photon density is the highest. For high numerical aperture objectives the excitation region is typically 0.3 microns in the radial direction and 0.9 microns in the axial direction. Excitation localization not only reduces cell damage and photobleaching, but also creates a 3-D sectioning effect. A further advantage of two-photon microscopy is excellent background rejection due to the excitation wavelength being widely separated from the emission light and thus it can be easily eliminated with filters.

Furthermore two-photon microscopy is particularly well suited for high-resolution studies of thick tissues and cells. The longer wavelength used in two-photon microscopy has a deep penetration depth and low phototoxicity compared to the conventional confocal microscopy. For many high-resolution tissue studies it is often the ideal technique to employ.

With this in mind, we have built a 3D SPT that utilizes the inherent 3D localization of two-photon excitation. The 3D SPT system we have developed has a frequency response at the video rate, an effective spatial resolution of less than 15 nm, and an axial range that is limited by the working depth of the objective.

2.Materials and Methods

2.1. Instrument

Figure 1 shows the experimental setup for the two-photon SPT experiments. The system is built around a Zeiss Axiovert 110 epifluorescent microscope (Carl Zeiss, Thornwood, NY). The excitation source is a Mira 900 Ti-Sapphire mode-locked laser that is pumped by an Innova 310 argon-ion laser (Coherent Inc., Palo Alto, CA). The excitation pulses from the Ti-Sapphire laser are 150 fs in duration at full-width-half-maximum and have a repetition rate of 80 MHz. A galvanometer x-y scanner (Cambridge Technology, Watertown, MA) directs the light into the microscope. A short pass dichroic mirror (Chroma Technology, Inc., Brattleboro, VT) reflects the laser light entering the microscope to the objective. To perform axial scanning we move the objective using a piezo 721.1 PIFOC microscope focusing drive and a E612.C0 amplifier to drive the piezo (Polytec PI, Costa Mesa, CA). The dichroic mirror in the microscope passes the fluorescence from the sample to the detection system that consists of a R7400 photomultiplier tube (Hamamatsu, Bridgewater, NJ) operating in photon-counting mode. A home-built PCI card in a PC controls both the x-y scanner and the z-stage, and in addition counts the pulses from the discriminator. The software used to control the PCI card and to collect and display the data is custom-written in C++.

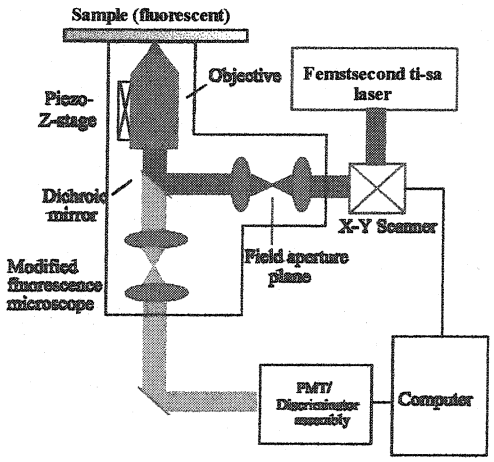

Figure 1: The standard setup for the two-photon microscope. Most of the modifications for particle tracking are software rather than hardware based with the exception of a signal-out from the scanner which servers to synchronize the start of the data acquisition with the software. This allows us to operate the scanner near it bandwidth-limited rate with greater accuracy.

2.2. Tracking Method

We have implemented two different techniques to accomplish 3D tracking on the two-photon microscope. The first method is use 3D volumetric scanning to localize the particle. The second technique is similar to Kao and Verkman's approach in that it utilizes aberrations in the PSF to determine the axial position of the particle.

There are three main ideas behind both of the techniques. The first is that the 3D sectioning effect of two-photon microscopy innately helps localize the axial position of the particle. The second idea is that by scanning only a small region in the vicinity of the particle we can achieve a higher frequency response than we could if we were scanning a larger area. And the third major idea is active feedback control in the tracking routine. As explained below, if the computer can calculate the position of particle and then quickly reposition the scan region, we can dynamically follow the motion of the particle over extended distances even though we are only scanning a small region at any given time.

In the volumetric tracking approach an x-y plane is built up pixel by pixel in the focal plane of the objective by scanning the laser beam with the galvanometer x-y scanning mirrors. The counts in each pixel are recorded by detecting the fluorescence with a photomultiplier tube operating in photon counting mode.

Immediately after scanning a plane, the axial piezo scanner repositions the objective and another x-y plane is scanned. The process repeats until we have built up sufficient volumetric information to determine the position of the particle. For this study we typically chose either three to six different axial positions. This was few enough to insure a sufficient frequency response, and many enough to allow an accurate determination of the axial position of the particle.

After acquiring a 3D volume the computer then calculates the location of the particle. For reasons of ease and computational efficiency, we have the computer perform a simple center of mass calculation to determine the particle's position within the volume. The computer then repositions the scan region by offsetting the origin of the new scan and place the particle in the center of the new scan region. As long as the procedure is fast enough such that the particle does not move outside the scan region while the volume is being scanned, it will be possible to dynamically follow the motion of the particle.

The other method we have implemented to track particles in three dimensions involves introducing aberrations that break the axial symmetry of the PSF into the optical system of the microscope. This symmetry breaking allows us to determine the full 3D position of the particle by merely scanning a single x-y plane in the vicinity of the particle.

We find that applying an uneven torque to the dichroic mirror in the microscope conveniently produces the needed aberrations by bending the mirror into a slightly cylindrical shape. Figure 2a is a plot of the PSF at several axial positions. The axial position of the particle is then determined from the shape of the PSF by calculating the generalized moment of the image, which is given by:

$$GM = \frac{(M_{yy} - M_{xx})}{(M_{yy} + M_{xx})} \tag{1}$$

where M_{yy} and M_{xx} are the second moments of the images:

$$M_{xx} = \frac{\sum_i x_i^2 \cdot I_i - \sum_i x_i \cdot I_i}{\sum_i I_i} \qquad M_{yy} = \frac{\sum_i y_i^2 \cdot I_i - \sum_i y_i \cdot I_i}{\sum_i I_i} \tag{2}$$

and x_i and y_i are the pixel position at the ith pixel, and I_i is the intensity at that position.

Figure 2b is a plot of the GM for the PSF pictured in 2a.

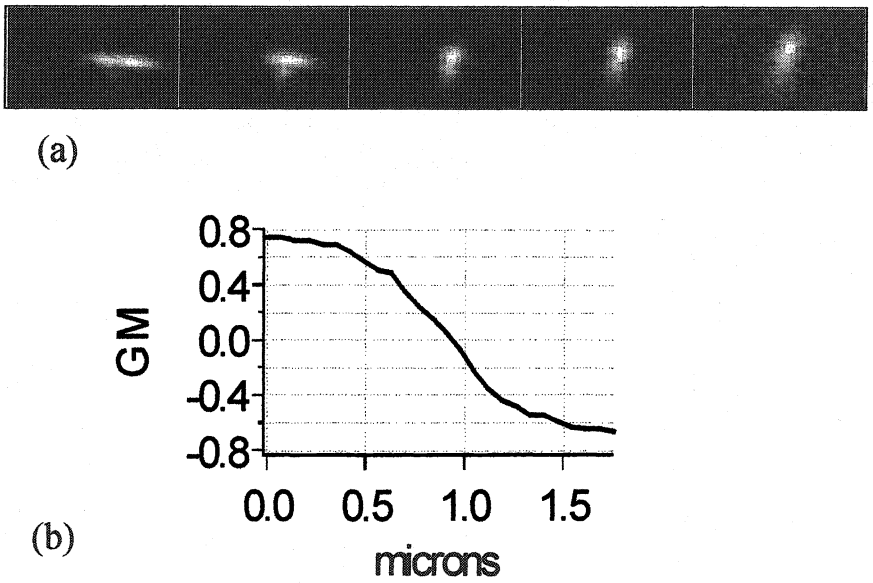

Fig 2: *(a) Successive axial images taken 750 nm apart of a 200 nm latex sphere embedded in an agarose gel taken with a C-Apochromat 40x water immersion objective. (b) The resulting GM curve for the central axial layers.*

When tracking the particle the radial position is determined by a center of mass calculation. To determine the axial position the computer calculates the GM of the image and then relates this back to the axial position of the particle by using the inverse of the GM versus distance curve show in 2b.

2.3. Computer Simulations

In order to test the theory for 3D SPT, we performed 3D random walks on both a lattice and continuum model. For the continuum model, we specify the distance the particle moves by generating a Gaussian random deviate of unit variance. Two uniform random deviates determined the azimuthal and radial angle of the particle motion. For the lattice model calculations, we chose a cubic lattice and generated a uniform random deviate to specify one of the six possible directions the particle could move at each step. All the random deviates were generated with the C routines gasdev and ran2 (Press et al., 1992).

For both of the models, we scaled the calculations using the relation:

$$l^2 = 6Dt \qquad (3)$$

2.4. Data Analysis

The aim of data analysis in SPT is to extract from a particle trajectory the relevant parameters that characterize the motion (such as the diffusion coefficient, velocity, and escape time), and then use this information to assign various modes of motion to the trajectory or sub-trajectory[10]. Some of the modes of motion investigated are free diffusion, diffusion with flow, and diffusion in environments where a particle can be trapped for a period of time before again diffusing away.

The difficulty in classifying trajectories is that a pure random walk can mimic a wide variety of motions. In many cases, it is not a trivial matter to make a conclusive categorization of even a simulated trajectory. Matters are made worse for

The difficulty in classifying trajectories is that a pure random walk can mimic a wide variety of motions. In many cases, it is not a trivial matter to make a conclusive categorization of even a simulated trajectory. Matters are made worse for experimental data due to the spatial and temporal limitations of the instrument and the finite length of the trajectories. To help classify the trajectories we will employ both MSD plots and statistical assays that quantify the probability that a particle with a known diffusion coefficient D stays within a certain radius R for all times t.

2.4.1. MSD versus Time Plots

The MSD plot for a trajectory of N points is given mathematically as

$$MSD_n = MSD_x(n\Delta t) + MSD_y(n\Delta t) + MSD_z(n\Delta t) \tag{4}$$

where

$$MSD_p(n\Delta t) = \sum_{i=0}^{N} (p_{i+n} - p_i)^2 \Big/ (N+1) \qquad p = x, y, z \tag{5}$$

and n is the lag time being considered. Thus for example, MSD_3 would be the average square distance a particle moved in three time steps.

There are two main types of motion with which we will be concerned with in this paper when dealing with MSD plots. They are represented mathematically by:

$$\langle r^2 \rangle = 6Dt \qquad \text{Normal Diffusion} \tag{6}$$

$$\langle r^2 \rangle = 6Dt + (Vt)^2 \qquad \text{Diffusion with flow} \tag{7}$$

To determine the diffusion coefficient of a particle, we have fit a straight line to the first three points of the mean square distance (MSD) versus time plot for the trajectory. If the entire MSD versus time curve is fit to find the diffusion coefficient, the resulting distribution of diffusion coefficients is so broad as to make the calculation useless[11]. The reason being is that there are fewer sub-trajectories of longer length in a trajectory, and thus there will be a greater variance in the value of the MSD for the longer lag times. This leads to a very broad distribution in the slopes of the fits to the MSD versus time plots. An alternative and frequently equivalent approach is to use a weighted fit to the MSD plot that gives greater weight to the shorter time lag points.

2.4.2. Transient Trapping of a Particle

Next we turn to methods to detect confinement of diffusing particles. The discussion will follow the work done by Saxton[12] and Simson et al [13]. who both dealt with the two-dimensional case.

In many instances in SPT it is necessary to distinguish between a trajectory that is a pure random walk and one that is constrained within a certain region. For example, one may wish to ascertain whether a receptor molecule is trapped within a microdomain in the plasma membrane, or whether a vesicle is trapped within a region in the cytoplasm. As noted in the last section, we can in principle solve the problem by plotting the MSD versus time. For a sufficiently long trajectory or ensemble of trajectories, the character of the motion will be evident by the shape of the curve. However, in cases where the particle undergoes transient trapping, or where there is only short trajectory available to examine, it is more complicated to establish whether the motion was the result of actually being trapped within a region or was merely due to Brownian motion.

Testing for the regions by merely visually inspecting the trajectory is unsatisfactory[12]. There are too many instances where a pure unobstructed random walk can mimic the motion of a confined particle. What is needed is a quantitative test to detect these trapping regions. Fortunately, such an assay to test for confinement in three dimensions has been derived previously in the literature. The probability that a particle with diffusion coefficient D remains within a region of radius R for all time t is proportional to:[14]

$$\Psi(R,t) = 2 \cdot \sum_{k=1}^{\infty} (-1)^k \exp(-\pi^2 k^2 Dt / R^2) \qquad (8)$$

We plot $\Psi(R,t)$ versus R in Figure 3 for various values of N. To test the theory, Monte Carlo calculations were performed for random walks. As seen from the Figure 3, the Monte Carlo calculations agree well with theory.

To aid interpretation, Simson *et al.* graphically represented $\Psi(R,t)$ as:

$$\xi = -\log(\Psi) - 1 \qquad \Psi \le 0.1$$

$$\xi = 0 \qquad \Psi > 0.1 \qquad (9)$$

$\Psi > 0.1$ is set to zero because we are only interested in identifying regions that have less that a 10% chance of being due to Brownian motion.

To rest for trapping we calculated an average value of ξ for each point in the trajectory and plot ξ versus the points in the trajectory. We use the same procedure that Simson et al.[13] used to calculate the value of ξ for a point. Higher values of ξ correspond to higher probabilities that the motion is not Brownian.

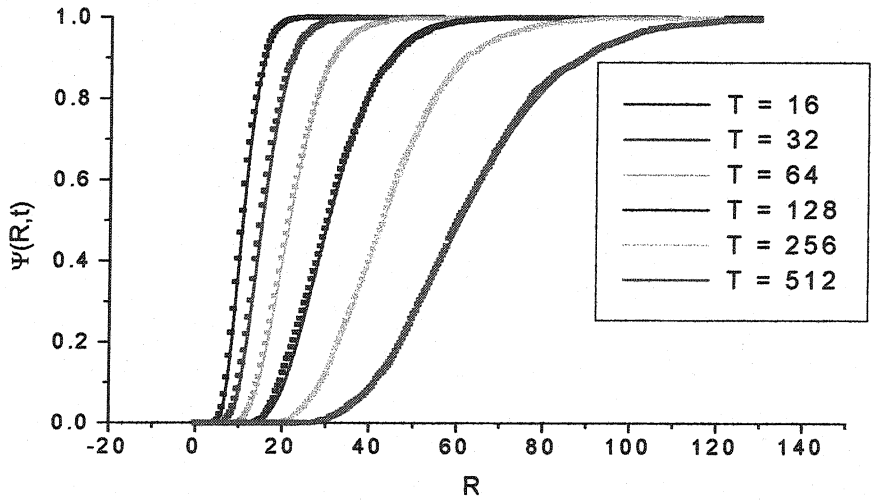

Figure 3: *Ψ(R,t) was plotted as a function of R for various values of t. Time t =16 is the furthermost trace on the left and t = 512 the furthermost trace on the right. The lines are the theory from Equation 8 and the dotted lines are the average results of 2048 Monte Carlo simulations conducted for each of the indicated times. A diffusion coefficient of one was assumed for the calculations.*

3.Results

3.1. Immobilized Sphere

To test the instrument we tracked immobilized 200 nm latex spheres that were dried on a coverslip (Figure 4). We obtained a standard deviation of approximately 30 nm in both radial directions and 40 nm in the axial direction. This is higher than what we would expect given the photon count rate for the particles, but is consistent with what we obtained with standard wide field video microscopy obtained on the same microscope. The optical table we performed these particular measurements on was not vibration isolated. This is what we think is causing the relatively high standard deviations. In figure 4b we measured the inter-particle distance of two particles as a function of time (which should be more independent of vibrations than the position measurement of a single particle) and obtained a standard deviation of 14 nm, which is more consistent with what we expect given the number of detected photons.

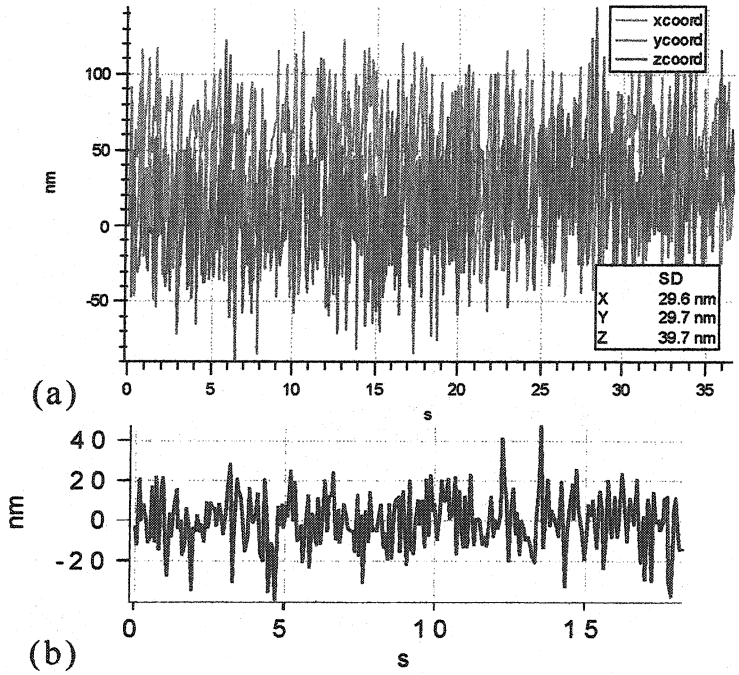

Figure 4: *Immobilized 200 nm spheres dried on a microscope coverslip. The objective was a Zeiss 63x oil immersion objective. (a) The time trace for each of the axis for a single particle. The standard deviation were 29.6 nm,29.7 nm, and 39.7 nm for x,y and z-axis. Note: the traces were slightly offset from one another. (b) The interparticle distance between two particles dried on a coverslip. The standard deviation of the measurement was 14.1 nm.*

3.2. Test Trajectories

To further test the instrument, we mounted a xy-piezo stage on the microscope (P-730 Piezo xy-scanner with E-612.C0 controller) in order to be able to move the sample in well-defined trajectories. The particular dataset shown in Figure 5 was obtained with the aberration method and with a frequency response of 14 Hz. We obtained similar results with other parameters. The piezo was mounted vertically such that the sample could be moved along the axial axis of the microscope system and along one of the radial axis. First we compared the trajectory we obtained by moving the sample along the same trajectory first along the y-axis and then along the z-axis. A 5 μm sine wave with a frequency of 0.1 Hz was input into the xy-piezo. This same input signal was then used to drive the other axis for comparison. The recovered trajectories were with 5% of the accepted axial calibration for the microscope system and had identical frequencies given the precision of the instrument as described in Figure 3. In Figure 5b we tested whether the amplitude of the motion would scale appropriately

by changing the amplitude of the input function. A 5 μm and 2 μm signal were separately input into the piezo, and the recovered motions were within 3.8% of one another. This is higher than what we would expect and is most likely due to the fact that the z-piezo used to drive the objective was operating in open-loop mode and the hysteresis of the piezo was not taken into account.

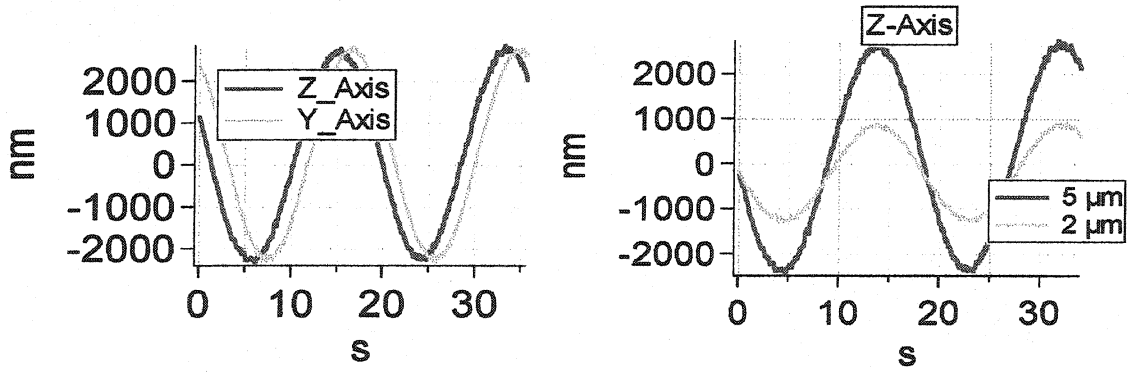

(a) (b)

Figure 5: *Recovered trajectories obtained from tracking a particle dried on a coverslip. The entire sample was mounted to a xy piezo scanner that could move the particle along both the z and y-axis independently. The input signals were sine waves from a function generator.*

3.3. Model Systems

We examined a number of other model systems in order to see if we could identify different modes of motion. To do this we tracked 200 nm latex spheres in sucrose solutions. The two types of motion we expect for trajectories free in solution are pure diffusion and diffusion with flow. Diffusion with flow will occur if the system contains convection currents; otherwise, we will have pure diffusion. Both modes of motion are mathematically well-characterized phenomena, so they make suitable systems to test the instrument. Sucrose solutions were used to increase the viscosity of the solutions relative to that of water. This was done so as to make the diffusion coefficients physiological and to further test the instrument by tracking particles over a range of diffusion coefficients.

Figure 6a shows a typical trajectory of particle tracked in 60% sucrose. The motion appears to be Brownian in all three dimensions. The data consisted of a sequence of 400 coordinates that were recorded 250 ms apart and were taken with the volumetric tracking approach. Figure 6b contains the MSD versus time plots of the trajectory of figure 6a. The resulting curves are very nearly the straight line we would expect from pure Brownian motion. The slope of the MSD for the individual axis is approximately one-third the slope of the radial MSD, which we expect for isotropic diffusion. The deviations from the straight line are due to the stochastic nature of the Brownian motion and are within the anticipated statistical fluctuations. Figure 6c shows the MSD plots for lag times up to 0.5 s. The recovered parameters from the linear fits are 4.13E-10 cm^2/s, 4.33E-10 cm^2/s, and 4.53E-10 cm^2/s, for the individual x, y, and z axis, and 4.30E-10cm^2/s for the overall diffusion coefficient.

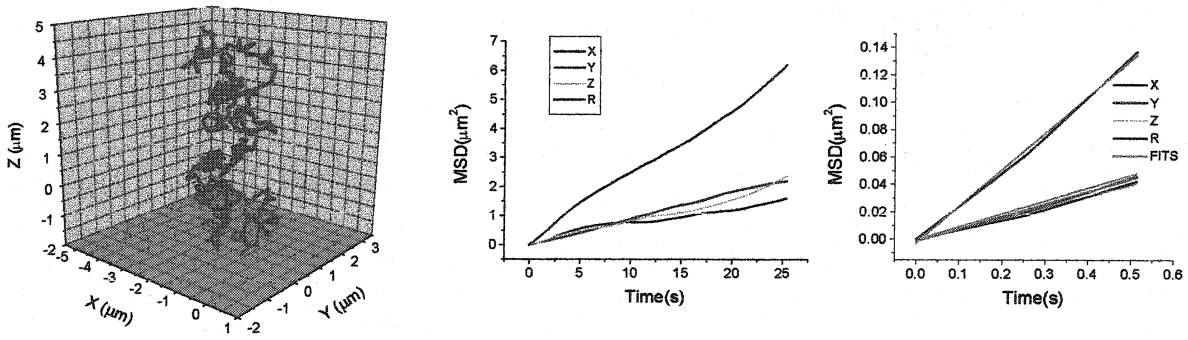

Figure 6: *200 nm sphere in 60% sucrose (a) 3D trajectory of the sphere (b) MSD versus time plot for lag times up to 25 seconds. (c) MSD versus time for lag times up to 0.5 seconds.*

The average recovered diffusion coefficient for 10 different trajectories of 200 nm spheres in 60% sucrose is 4.1E - 10 cm^2/s. This is within 10% of the value of 3.8E-10 cm2/s we expect from the Stokes-Einstein relationship given by:

$$D = \frac{kT}{6\pi\eta R} \tag{10}$$

where k is Boltzmann's constant, T is the temperature (295 K), R is the radius of the particle, and η is the viscosity of the solution.

Figure 7a shows an example of diffusion with flow. The sample consisted of 200 nm spheres in a 50% sucrose solution. This sample was less viscous than the 60% sucrose solution and had greater convection currents. The data consisted of a sequence of 1000 coordinates that were recorded 125 ms apart and was obtained using the volumetric tracking approach. To obtain the diffusion coefficient we fit a straight line to the first three points of the trajectory as shown in Figure 7c. The recovered value of 14.4E-10 cm^2/s was within 2% of the expected value as determined from the Stokes-Einstein relation. To calculate the velocities, we fit the trajectory to equation 5, with D and V as parameters. The fit is shown in Figure 7b. The recovered speeds for the flow were 0.35 µm/s, 0.24 µm/s, and 0.19 µm/s for the x, y, and z-axis respectively, and 0.467 µm/s for the overall speed. Caution must be exercised in the interpretation of the velocity parameters. We assumed uniform flow over the entire length of the trajectory, which may not be a valid assumption since the velocity could have been changing in this interval. This is a general concern when trying to apply the model of pure diffusion with flow to experimental trajectories. One way to address the problem is to break the trajectory into shorter segments and analyze each segment separately. The velocity in each segment would then more likely be constant. At any rate, the velocities that were recovered by the fit are reasonable given the dynamics of the system.

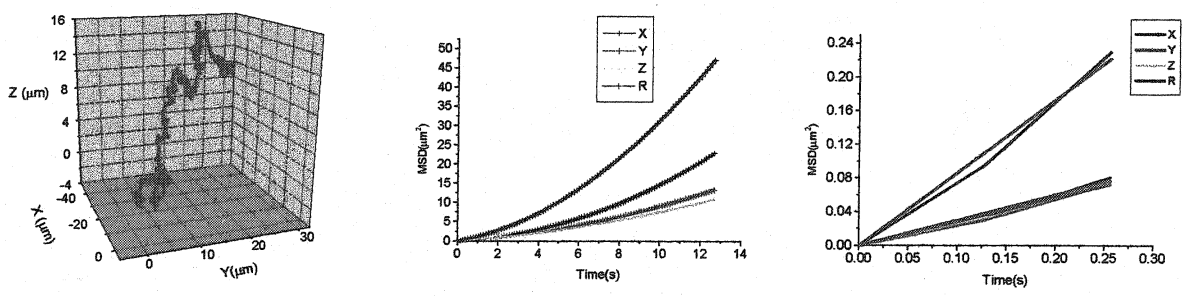

(a) (b) (c)

Figure 7: *200 nm sphere in 50% sucrose (a) 3D trajectory of sphere. (b) MSD versus time plot for lag times up to 0.25 seconds. (c) MSD versus time for lag times up to 12.5 seconds.*

Figure 8 is a plot of recovered diffusion coefficients for particles tracked in 60%, 56%, 50%, and 40% sucrose using the volumetric scanning method. The diffusion coefficients were plotted versus inverse viscosity. The resulting fit is linear as expected from the Stokes-Einstein relationship, and has a slope of 2.09 N which is within 3.3% of the value of 2.16 N we expect for the conditions of the experiment.

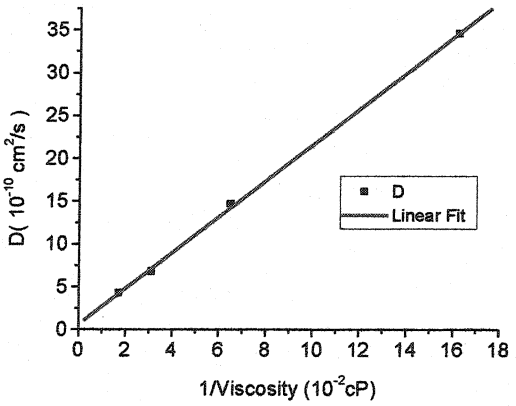

Figure 8: *Recovered diffusion coefficients for 60%, 50%, 56%, and 40% sucrose solution as a function of viscosity. The graph shows the expected linear relationship predicted by the Stokes-Einstein equation.*

We also tracked the motion of latex spheres in 0.3% agarose gels. Agarose gels consist of a network of cross-linked polymers that, on the microscopic scale, form an inhomogeneous media with pores of different sizes that can transiently trap a diffusing particle.

Figure 9 shows the some of the results obtained from tracking a sphere in agarose. The data for the agarose experiments consisted of a sequence of 400 points each 256 ms apart obtained with the volumetric approach. The ξ-profile plot for the trajectory of the particle in the agarose gel was plotted in Figures 9b. The ξ-profile plots for the sphere in the agarose gels display significant trapping. The ξ value of 32 in Figure 9b corresponds to only a 1E-33 probability that the motion of the particle in this region was due to pure Brownian motion.. In comparison, the ξ-profile plots in Figures 9c for a particle in 60% sucrose did not display any significant trapping with the highest ξ value being only 1.2. This is consistent with our earlier classification of the motion of 200 nm spheres in 60% sucrose as pure Brownian motion.

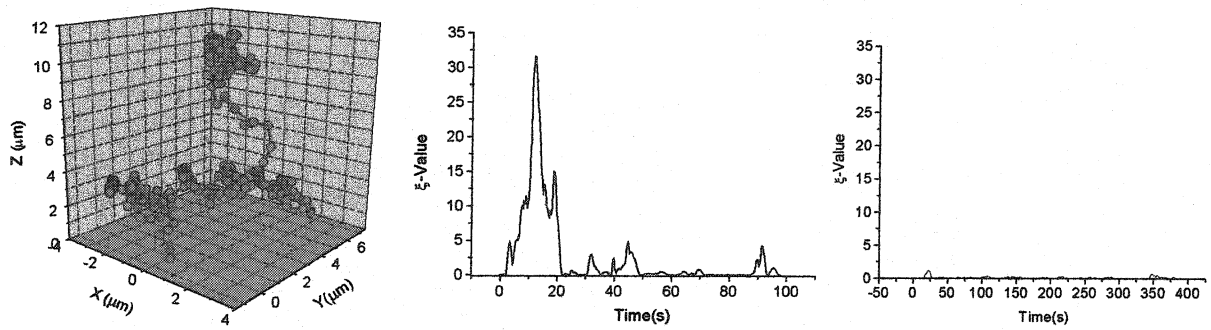

(a) (b) (c)

Figure 9: *(a) 3D trajectory of a 200 nm spheres in a 0.3% agarose solution. (b) ξ-Profile plots for (a). The particle started at the origin and was trapped in a microdomain for approximately 20 seconds, and then was trapped twice more between 30 and 50 seconds into the trajectory and again at approximately 90 seconds. (c) For comparison, the profile plots for 200 nm spheres in 60% sucrose from Figure 6. No significant tracking was observed as is expected.*

4.Discussion

We have constructed a novel SPT instrument that simultaneously tracks particles in all three dimensions using two different but related techniques. The volumetric scanning approach has a frequency response of up to approximately 6-8 Hz and is very straightforward to implement. The aberration method allows us to track particle in all three dimensions at a currently maximum rate of approximately 28 Hz. We tested the instrument by moving the sample in well-defined trajectories with a xy piezo scanner attached to the microscope and tracking the particle with the techniques. We also investigated different methods that can help classify the 3D trajectories we obtain from various modes of motion. The diffusion coefficients recovered for 200 nm latex spheres in solution were in agreement with the Stokes-Einstein relation, and the standard deviation in the distribution of diffusion coefficients were within what we expected given the statistical and instrumental uncertainties of the method. None of the trajectories in the free solution displayed any trapping as determined by the plots of their ξ-profiles. In contrast, the motion of the spheres in the agarose gel did display significant trapping. The data we have obtained so far are all self-consistent and establishes that the basic methodology we have developed is sound.

The technique can be improved in a number of relatively easy ways. First, the galvanometer scanner we are using is an older model and is bandwidth limited to 500 Hz. Current scanners can go as fast 1 kHz, which will gives us a factor of two increase in performance and allow us to track particles at 60 Hz. Second, the dichroic we used to generate the aberrations in the aberration tracking method can be fabricated to a specific curvature. This may allow us to extend the range over which we can ascertain the 3D position of the particle without having to reposition the objective. Also, specifically engineering a PSF may allow us to increase the precision of the axial position measurement. Thirdly, we can incorporate simultaneous wide-field imaging, which will allow us to monitor the position of the particle relative to any larger structures of interest. This would be of particular interest where the global structure of the sample is also changing, such as in cell migration studies.

5.Conclusions

We have developed a SPT system on the two-photon microscope that is capable of tracking a particle in all three dimensions over an extended axial range at a fast frequency response. The system is built around a two-photon fluorescence microscope and utilizes the inherent 3D localization of two-photon excitation. We have studied the motion of particles in model systems consisting of sucrose solutions and agarose gels. We have been able to extract the relevant parameters that characterize the trajectories and classify the mode of motion as either pure diffusion, diffusion with flow, or transient trapping.

6.Acknowledgements

We would like to acknowledge NIH grants RR03155 to E.G. and R29GM56486-01 to P.T.S.

7.References

[1] Barak, L., Webb, W. 1982, Fluorescent Low Density Lipoproteins for Observation of Dynamics of Individual Receptor Complexes on Cultured Human Fibroblasts, *J. Cell Biol.*, **90**, 594-604.

[2] DeBrabander, M., Geuns, G., Nuydens, Moeremans, M., and J. DeMey, 1985, Probing microtubules-dependent intracellular motility with nanometer particle video ultramicroscopy (nanovid ultramicroscopy), *Cytobios*, **43**, 273-283.

[3] Gelles, J., Schnapp B.J., Sheetz, M.P., Tracking kinesin-driven movements with nanometer-scale precision, *Nature*, **331**, 450-453.

[4] Schmidt, Th., Schutz, G.J.,Baumgartner, Gruber, H.J., Schindler, H., 1996, Imaging of single molecule diffusion, *Proc. Natl. Acad. Sci.*, USA, **93**, 2926-2929.

[5] Simson, R., Yang, B.,Moore, S.E., Doherty, R.,Walsh, F.S., Jacobson, K.A., Structural Mosaicism on the Submicron Scale in the Plasma Membrane, *Biophys J.*, **74**, 297-308.

[6] Kao, H.Pin, and A.S. Verkman, 1994, Tracking of Single Fluorescent Particles in Three Dimensions: Use of Cylindrical Optics to Encode Particle Position, *Biophys. J.*, **67**, 1291-1300.

[7] Peters, Inge M., de Grooth, B.G., Schins, J.M., Figdor, C.G., and Jan Greve, Three dimensional single particle tracking with nanamoter resolution, *Review Sci. Instruments*, **69**, 2761-2766.

[8] Pralle, A., Prummer, M., Florin, E.L., Stelzer, E.H.K., and Horber, J.K.H. Three Dimensional High-Resolution Particle Tracking for Optical Tweezers by Forward Scattered Light. *Microscopy Research and Technique,* **44**, 378-386.

[9] Denk, W., J.H. Strickler and W.W. Webb, 1990. Two-photon laser scanning fluorescence microscopy, *Science*, **248**, 73-76.

[10] Saxton, M.J.,Jacobson, K.,1997, Single Particle Tracking: Applications to Membrane Dynamics, *Ann. Rev. Biophys. Biomol. Struct.*, **26**,373-399.

[11] Saxton, M.J., 1997, Single-Particle Tracking: The Distribution of Diffusion Coefficients, *Biophys. J.*, **72**, 1744-1753.

[12] Saxton, M.J., 1993, Lateral diffusion in an archipelago: single particle diffusion, *Biophys. J.* **64**,1766-1780

[13] Simson, R., Sheets, E.D., and K. Jacobson, 1995, Detection of Temporary lateral confinement of Membrane Proteins Using Single Particle Tracking Analysis, *Biophys J.*, **69**, 989-993.

[14] Rubin, R. J., Mazur, J., and G. H. Weiss Spans of Polymer Chains, *Pure & Appl. Chem.*, **46**, 143-148.